Quasiperiodic transition to spatiotemporal chaos in weakly ionized magnetoplasmas

J. H. Chu and Lin I
Department of Physics, National Central University, Chungli, Taiwan 32054, Republic of China
(Received 14 June 1988)

The transition to temporal and then spatiotemporal chaos in a weakly ionized magnetoplasma system which supports nonlinear flute-type ionization-drift waves was studied. The system is similar to a reaction-diffusion system with additional drift-induced transverse spatial coupling. It follows a complex quasiperiodic route with strong nonlinear mode-mode competition, a narrow frequency-locking interval, and an unstable third independent frequency to temporal chaos. At the onset of the spatial chaos, the discrete spatiotemporal modes decrease down to the noise floor, the temporal correlation reduces more than ten times, and the correlation dimension jumps from less than 8 to greater than 12.

I. INTRODUCTION

Drift waves exist in various collisional and collisionless magnetoplasma systems such as Penning discharges, Q machines, tokamaks, magnetron discharges, etc.[1–7] They have been of fundamental interest in the traditional study of turbulence and anomalous transport in plasmas. The magnetoplasma is a nonlinear continuous dissipative system with many degrees of freedom and additional spatial coupling induced by the Lorentz-force and spatial inhomogeneity. Along with the recent intense researches of order and chaos in many nonlinear physical systems, the drift-wave system becomes an interesting subject for testing the universal characteristics of chaos such as the low-dimensional behavior and certain routes to chaos which have been found in other nonlinear systems, e.g., reaction-diffusion systems, hydrodynamic systems, solid-state plasmas, nonlinear optics, etc.[8–15] It also makes possible the study of the transition to spatial chaos and the spatiotemporal relationship which has not been fully explored in other nonlinear physical systems. In recent computer simulations, different routes to chaos (Hopf bifurcation sequence and Feigenbaum period doubling) were found by Biskamp and Kaifen[3] and Terry and Horton[4] for drift-wave systems. However, to the authors' knowledge, no detailed experimental study of the chaotic behavior for drift-wave systems has been carried out, in particular, for a weakly ionized magnetoplasma in which an additional ionization process plays a role similar to the reaction process in a chemical system.[6–9] This paper presents the experimental study of the nonlinear phenomena and transition to temporal and then two-dimensional spatial chaos in a weakly ionized rf magnetron system which supports large-amplitude nonlinear ionization-type drift waves. A complex quasiperiodic transition to temporal and then spatiotemporal chaos was observed, with nonlinear competition between two resonance modes and a narrow frequency-locking interval. The unstable regime in the parameter space, the correlation dimensions of the attractors, and the spatial and temporal correlation of the chaotic fluctuations were investigated.

The fundamental principle of the nonlinear drift waves in a weakly ionized ($<1\%$) low-pressure (~ 10 mTorr) magnetoplasma ($B\sim$ 100 G) can be found elsewhere.[5–7] The discharge for the experiment is sustained in a cylindrical magnetron system by stationary rf input power. It supports a strong electron-density gradient and electric field adjacent to the system boundary.[7] Electron motion can be affected by the moderate magnetic field due to its small mass. Ions only respond to the low-frequency density gradient and space-charge field. The electron $E\times B$ and diamagnetic drifts due to the coupling between the Lorentz force and spatial nonuniformities cause charge separation, and in turn drive the well-known drift waves propagating normal to the magnetic field. The ionization rate is proportional to the local electron density. The ionization process in the partially ionized discharge further provides a positive feedback to enhance the density fluctuation.

Neglecting charge-charge collision and volume recombination in the low-density plasma, the continuity equation of electron density follows:[7]

$$\partial n_e/\partial t = D_{ejk}\nabla_j\nabla_k n_e - \mu_{ejk}V_j(n_e\nabla_k\phi) + Zn_e \ , \tag{1}$$

$$D_e = (T_e/m_e\nu_{e0})\begin{bmatrix} r^2 & r & 0 \\ -r & r^2 & 0 \\ 0 & 0 & 1 \end{bmatrix} , \tag{2}$$

$$r = \nu_{e0}/\omega_{ce} \ll 1 \ , \tag{3}$$

$$\mu_e = (e/T_e)D_e \ , \tag{4}$$

where n_e is the electron density, $\nabla_k = \partial/\partial x_k$, ϕ is the space-charge potential, r is the ratio of the electron-neutral collisional frequency ν_{e0} to the electron gyrofrequency ω_{ce}, T_e is the electron temperature, and Zn_e is the source term due to electron-impact ionization. Other conservation equations of momentum and energy also have similar structure for the spatiotemporal coupling. Along with the Poisson equation, they form a set of coupled nonlinear partial differential equations which determine the spatiotemporal evolution of the system. Generally, the electron-impact ionization is similar to a reaction process which enhances the temporal density fluc-

tuation. The diagonal transport terms are controlled by the electron-neutral collisional process, and cause dissipative spatial coupling. The off-diagonal transports in the diffusion and mobility terms correspond to the diamagnetic drift and $E \times B$ drift. They are almost nondissipative under the low pressure, and provide rotational convective coupling in the plane normal to the magnetic field, namely, a weakly ionized magneto-plasma system shares some common features with a chemical-reaction–diffusion system in which chaos has been observed,[8,9] but with an additional space-charge field and transversed nondissipative transport for spatial coupling.

II. EXPERIMENT

The experiment was performed in a cylindrical rf magnetron system. The experimental setup is similar to the other magnetron system with an oval cross section.[7,16] As shown in Fig. 1, the system consisted of two 30-cm-long concentric cylindrical stainless-steel electrodes with 2.5- and 8-cm diameters, respectively. The center one was grounded and the outer one was capacitively coupled to a rf power amplifier (ENI A-500) which was driven by a Philipps PM 5193 programmable function generator with frequency fixed at 14 MHz. The system is initially evacuated to 10^{-6} Torr and operated above 1 mTorr. Ar gas was used. A uniform moderate axial magnetic field (< 100 G) was generated by two solenoids. A weakly ionized low-temperatured steady-state rf discharge ($n_e \sim 10^{11}$ cm^{-3} and $T_e \sim 5$ eV) was sustained between the electrodes. The discharge has excellent axial uniformity. Radially, the discharge can be divided into nonuniform dark space regions adjacent to the electrode surfaces and a glow region.[16] The former are about 2 mm thick and support a large density gradient and a strong rf-induced dc electric field. Electron-density fluctuations were measured simultaneously by two Langmuir probes 7 mm away from the outer electrode surface and separated 12° (6.9 mm) azimuthally. Probes were biased such that the normalized electron current fluctuations were independent of the bias potential. Signals were digitized by a Hitachi VC 6041 digital scope, and processed by an IBM personal computer.[6,7]

The state of the discharge is a complicated function of

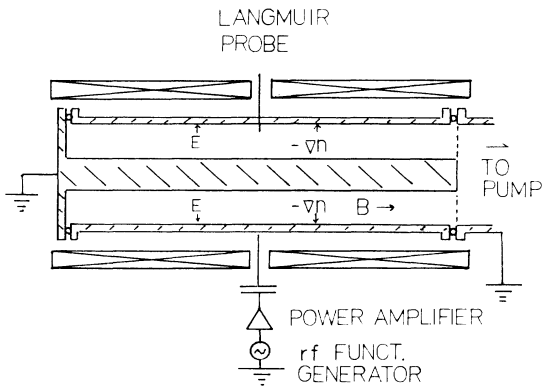

FIG. 1. Side view of the cylindrical rf magnetron system.

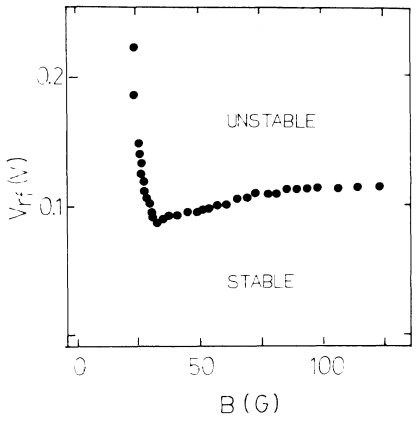

FIG. 2. V_{rf}-B phase diagram for the onset of f_1 oscillation in a 3-mTorr argon discharge.

several system operating parameters such as rf power, gas pressure, magnetic field strength, gas chemistry, system size, etc.[7,16] For simplicity, the amplitude of the rf driving signal V_{rf} from the programmable function generator, which controls the rf input power (rf input power proportional to V_{rf}^2 and power of 44 W at $V_{rf}=0.20$ V), was chosen as a control parameter leading the system to turbulence. Increasing rf power increases the ionization rate, plasma density, and the zeroth-order spatial inhomogeneity adjacent to the system boundary, namely, increasing rf power enhances the reaction, drift, and diffusion processes, and in turn leads the system to turbulence. The digital function generator allows 0.001 V minimum step for the variation of V_{rf}. The ratio of the magnetic field strength to the system pressure controls the spatial coupling and forms another important control parameter.[5,7] Figure 2 shows the measurement of the onset of the single-mode oscillation on the V_{rf}-B phase diagram at 3 mTorr. It has rich chaotic structure in the unstable region. In this paper we report the transition to chaos by varying V_{rf} in a 50-G 3-mTorr argon discharge. The effect of the magnetic field strength will be reported in the near future.

III. RESULTS AND DISCUSSION

Figures 3 and 4 show the transition to temporal chaos as we vary V_{rf}. Basically, it follows a complex quasi-periodic route with regular windows, two regions with different fundamental frequency modes, frequency ratio locking, and strong nonlinear interactions.

For $0.096 \text{ V} < V_{rf} < 0.103$ V [Fig. 3(a)], the plasma shows regular oscillation with $f_1 = 273$ kHz and its harmonics. At $V_{rf}=0.104$ V [Fig. 3(b)], a large-amplitude ($\Delta I/I \sim 1$ low-frequency oscillation with an incommensurate fundamental frequency $f_2 = 25$ kHz and mode number $m = 1$ suddenly sets in. The mode number was obtained by comparing the phase difference of the Fourier-transformed signals from the two adjacent probes. The high-frequency oscillations are strongly amplitude as well as frequency modulated by the low-frequency fluctuations. The amplitude and the period of

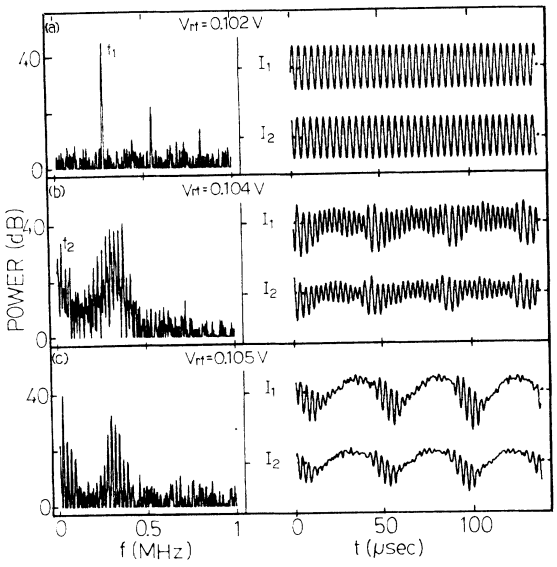

FIG. 3. Power spectra and oscillatory currents (ac coupled, and electron density $\propto -I$) from two probes separated 12° azimuthally ($B=50$ G and $P=3$ mTorr). $\mathbf{r}_{21}=\mathbf{r}_2-\mathbf{r}_1$ is along the diamagnetic drift direction.

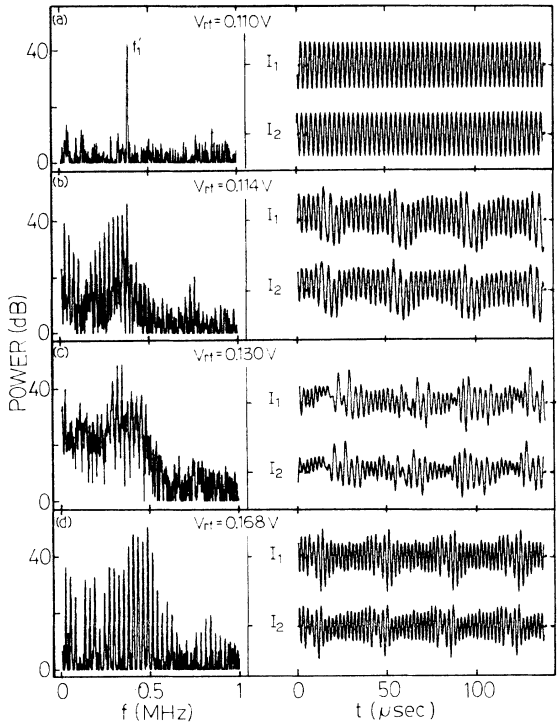

FIG. 4. Power spectra and oscillatory probe currents as in Fig. 3 except at different V_{rf}.

the high-frequency oscillation both increase with the electron density (note that $n_e \propto -I$). The power spectrum shows two regions of equally separated sharp peaks with $f=n_1 f_1+n_2 f_2$ and $n_1=0$ and 1 for those regions, respectively. The high-frequency and the low-frequency modes compete with one another for $0.104\text{ V} < v_{rf} < 0.110$ V. As V_{rf} increases from 0.104 V, the relative strength of the high-frequency part first decreases [Fig. 3(c)] and then increases.

As V_{rf} increases to 0.110 V [Fig. 4(a)], the strength of the low-frequency oscillation goes down to the noise level and the system returns to an almost single-mode high-frequency oscillation again with a new $f_1'=382$ kHz. This single-mode oscillation only exists in a very narrow window ($\Delta V_{rf}<0.001$ V). For $0.110\text{ V} < V_{rf} < 0.200$ V [Figs. 4 and 5(a)], the two incommensurate modes and their sideband modes due to nonlinear competition reappear. f_1 and f_2 both vary with V_{rf}. The plasma is driven to a more chaotic state and the relative strength of the continuous background increases with increasing V_{rf}, except in a narrow window ($\Delta V_{rf}=0.005$ V) in which frequency ratio locking occurs. For example, at $V_{rf}=0.114$ V [Fig. 4(b)], amplitude and frequency modulations similar to Fig. 3(b) with $f_2=25.39$ kHz and $f_1/f_2=14.88$ were observed. However, a state such as that of Fig. 3(c) with large-amplitude low-frequency fluctuations has never occurred again. $\Delta I/I$ drops down to about the 20% level.

In the window around $V_{rf}=0.168$ V [Fig. 4(d)], f_1 and f_2 become rational. The spectrum shows large-amplitude equally separated sideband modes with frequency $f=nf_2$ and $f_2=27.07$ kHz. The pattern almost repeats itself after 17 times of the intrinsic oscillation. The frequency locking strongly suppresses the continuous background in the power spectrum to the flat instrumentation noise level. Similar frequency locking has been observed in other studies.[3,10,12] It is interesting that modes with $n=4$ and 8 have very weak strength. It should be noted that, for spectra with better resolution, a low-frequency mode $f_3=6.8$ kHz can be distinguished accompanying the rising continuous background after the onset of the temporal chaos. The strength of f_3 is at least 20 dB smaller than those of f_1 and f_2 at $V_{rf}=0.114$ V. It grows rapidly with V_{rf} and introduces splitting for

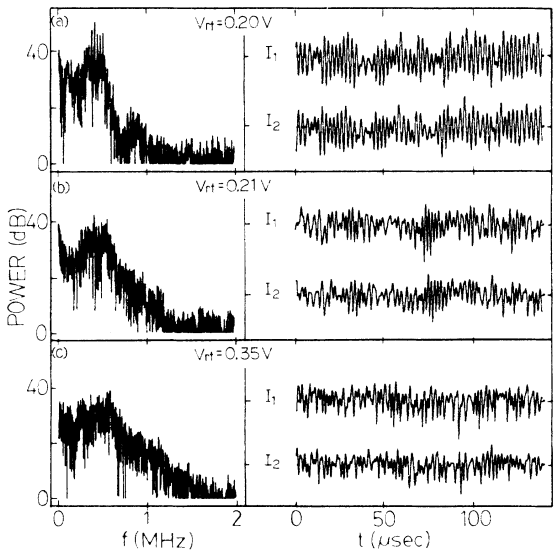

FIG. 5. Power spectra and oscillatory probe currents as in Fig. 3 except at different V_{rf}.

those sharply peaked modes through the nonlinear interaction processes. The fine splittings eventually merge together due to the broadening by nonlinear interaction and dissipation at high V_{rf}.

For $V_{rf}<0.20$ V, the signals from the two probes separated 12° azimuthally almost have the same structure [Figs. 3, 4, and 5(a)]. Figure 6 shows the cross correlation

$$C_{\Delta r}(T)=\langle I_{r_i}(t)I_{r_j}(t-T)\rangle/[\langle I_{r_i}(t)\rangle^2\langle I_{r_j}(t)^2\rangle]^{1/2}$$

between the signals from the two probes located at r_i and r_j. Their spatial coherence $C_{\max}$ [here it is defined as the maximum value of $C_{\Delta r}(T)$] remains about 0.94 ± 0.02 (Figs. 6 and 8) with coherence time greater than 50 μsec for $V_{rf}<0.20$ V. The fluctuations propagate against the electron diamagnetic drift direction with velocity ($\sim 0.5\times 10^6$ cm/sec) about the same as the electron diamagnetic drift velocity. At $V_{rf}=0.21$ V [Fig. 5(b)], we see the onset of the spatial chaos. The spatial coherence between the above two probes drops down to 0.7 (corresponding to the spatial coherence length <1.5 cm) and the fluctuations reverse their propagating direction. It is hard to identify the corresponding high-frequency fluctuations for signals taken from two probes separated 30°. At the onset of spatial chaos [$V_{rf}=0.21$ V, Fig. 5(b)], those equally spaced high-frequency spikes which are 10–15 dB higher than the continuous background in the power spectrum at $V_{rf}=0.20$ V [Fig. 5(c)] become indistinguishable; the power spectrum basically shows two broadband noisy bumps and a typical turbulentlike high-frequency tail with power strength $S(f)\propto f^{-n}$ [$n=5.5$ for Fig. 5(b)]. These two bumps gradually merge together and the system becomes fully turbulent when we further increase the rf power [Fig. 5(c)]. The coherent time of the fluctuations drops from greater than 50 μsec to a few microseconds at the onset of the spatial chaos (Fig. 6). Similar to the previous experiment,[6,7] the fluctuation still has excellent spatial coherence along the magnetic field. The spatial chaos is only two dimensional and inhomogeneous in the plane normal to the magnetic field.

Figure 7 shows the phase portraits and Poincaré sections constructed from the delayed-time series $I(t_i)$ at different V_{rf}. $I(t_i+T)$ versus $I(t_i)$ with $T=0.625\times 10^{-6}$ sec was plotted for the phase portraits. The Poincaré sections were cut along 135° and magnified 2.5 times from the phase portraits. Figure 7(b) shows the torus starts to collapse due to the nonlinear competition. For the case of frequency ratio locking [Fig. 7(c)], the trajectories concentrate in many fixed regions. The trajectories become more spread out as the system becomes more chaotic. It should be pointed out that the two opposite Poincaré sections (cut along 45° and 135°) are still distinguishable at $V_{rf}=0.20$ V; the onset of spatial chaos causes the mixing of the two opposite Poincaré sections.

The correlation dimension d of the attractor is measured according to the correlation method suggested by Grassberger and Procaccia,[17] based on the idea that the averaged number of points $N(r)$ in a ball of radius r scales with the dimension d, $N(r)\propto r^d$, in an m-dimensional inbedded phase space constructed by n equally sampled time series with interval T. The details have been described elsewhere.[6] Similar to the previous experiment,[6] n and T are properly chosen and tested such that d saturates with n and T. We got very good convergence of d using 1000 points and $T=0.5\times 10^{-6}$sec ($1/Tf_1\sim 5$ and $1/Tf_2\sim 80$) for the temporal chaos. d increases slowly with V_{rf} to 7.6 before the loss of spatial coherence (Fig. 8), except that in the regular windows it drops back to equal or less than 2. The results are very reproducible and the error bar is less than 5%. The onset of the spatial chaos causes the slowdown of the saturation of d as m increases, and a jump of d to greater than 12. For example, d increases fast to 10 at $m=40$ and then slowly increases to 12 at $m=80$ for $V_{rf}=0.21$ V. In contrast to a random noise system which usually needs large n for the convergence of d, d converges well in terms of the number of data points n (for $n>500$) for the tur-

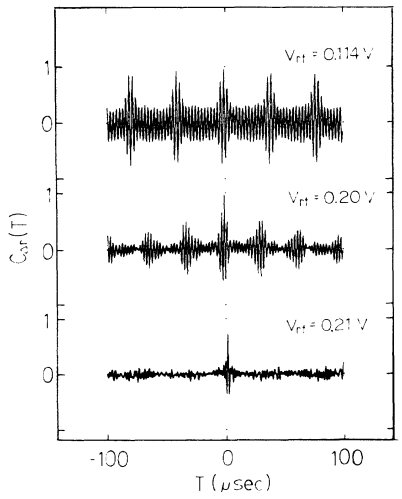

FIG. 6. Cross correlation $C_{\Delta r}(T)$ vs T at different V_{rf} with $\Delta\mathbf{r}=\mathbf{r}_i-\mathbf{r}_j$ and $\Delta\mathbf{r}\|\nabla n\times B$.

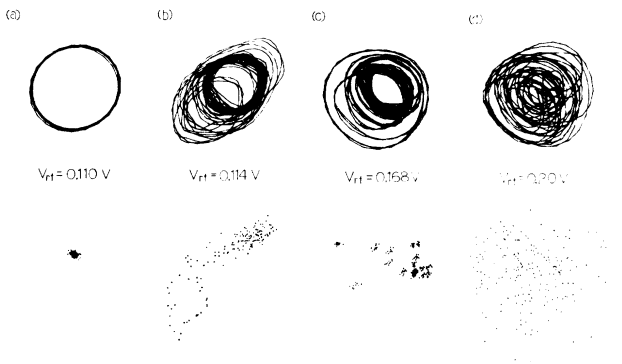

FIG. 7. Phase portraits $I(t+T)$ vs $I(t)$ and the Poincaré sections of the attractors at different V_{rf}, where $T=0.625$ μsec and the Poincaré sections are cut along 135°.

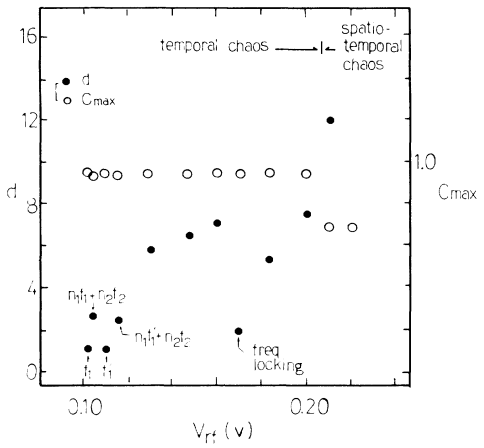

FIG. 8. Spatial correlation C_{max} between the 12° separated probe signals and the correlation dimension d vs V_{rf}.

bulent states in our system.[6] Although there have been some doubts about the significance of the correlation dimension under large inbedding dimension and small n, our measurement at least gives a lower bound of d at the onset of spatial chaos. The behavior of the spatial chaos and its correlation dimension are consistent with our previous experimental results in the oval magnetron and are discussed elsewhere.[6,7]

Our system is similar to a chemical-reaction–diffusion (CRD) system described by the time-dependent Landau-Ginzberg equation,[8,9] but with additional drift-induced transport for the transverse spatial coupling. A quasiperiodic transition with a frequency-locking window to chaos has been observed in CRD systems.[8,9] The observation of the two incommensurate modes, nonlinear interaction, frequency locking, and the intimate connection between the appearance of the third discrete frequency and the broadband noise in our system give another example of the quasiperiodic picture in spite of the extra transverse spatial coupling.[9,10,14] A similar quasiperiodic route to chaos was also observed in the computer simulation by Biskamp and Kaifen for a drift-wave system using a model of three-wave interaction and ten independent dynamical variable truncations, in which the system also encounters two different 2-tori as the control parameter varies.[3] This is in contrast to the period doubling route realized in the simulation using a low-order (four independent variables) dynamical system by Terry and Horton for drift waves.[4] Our chaos also exhibits hysteresis behavior in certain regions of V_{rf}, which was not predicted by Biskamp and Keifen.[3] Similar to other nonlinear systems, nonlinear frequency locking and Arnold tongue structure were observed in our recent experiment, when our system was driven by a probe with external sinusoidal voltage. The details of hysteresis and nonlinear frequency locking will be reported shortly.

Our system is a continuous system which potentially has an infinite number of degrees of freedom. The small correlation dimension before the onset of the spatial chaos manifests that only a small number of relevent degrees of freedom are excited and has also been observed in other systems.[11–13] In the absence of strong nonlinear interaction, the wave numbers of these spatially coherent modes must be quantized and commensurate under the cylindrical boundary condition. The incommensurate frequencies of the quasiperiodic modes are allowed by the slightly nonlinear dispersion relation observed by comparing the phase difference of the spectra from two adjacent probes. As a stationary open system, the levels of excitation, nonlinear interaction, and dissipation all increase with rf power. Under large V_{rf}, the strong nonlinear interaction and dissipation drastically change the lifetime of the discrete modes and relax the constraint on wave numbers set up by the boundary condition. More degrees of freedom can be excited. These are evidenced by the sudden jump of the correlation dimension and the reduction of the temporal and spatial coherence at the onset of spatial chaos. The observation of the suppression of the discrete modes, and the rising and broadening of the continuous background in the power spectra also give good support. Similar behavior of the jump of the correlation dimension at the onset of spatial chaos has also been observed in the electron-hole solid-state plasma and the channel flow turbulence.[12]

IV. CONCLUSION

We have observed a complex quasiperiodic transition to temporal and then two-dimensional spatial chaos in our weakly ionized magnetoplasma system as we varied the rf power. Our system is a nonlinear continuous dissipative system and combines the nature of the chemical-reaction–diffusion system and the drift system. Its dynamics can be described by a complicated set of reaction-diffusion-type partial differential equations with off-diagonal transport terms. Electron drift provides nondissipative rotational transverse spatial coupling in addition to the collisional dissipative transport. The observation of the low-dimensional attractor, quasiperiodic transition to temporal chaos, strong nonlinear mode-mode competition, a very narrow frequency-locking window with low noise, and the third unstable mode manifest that the universal characteristics of chaotic systems are followed in spite of the additional transverse spatial coupling and the complexity of the discharge system. Under large rf power, the excitation, strong nonlinear interaction, and dissipation significantly reduce the spatiotemporal coherence, allow a large jump of the correlation dimension, and lead the system to turbulence.

ACKNOWLEDGMENT

This work is supported by the Department of Physics, National Central University and The National Science Council of the Republic of China, Contract No. NSC 76-0208-M008-20.

[1]W. Horton, in *Handbook of Plasma Physics*, edited by M. N. Rosenbluth and R. Z. Segdeev (Elsevier, New York, 1984), Vol. 2, p. 383.
[2]For example, F. F. Chen, *Introduction to Plasma Physics* (Plenum, New York, 1977), Chap. 5.
[3]D. Biskamp and H. Kaifen, Phys. Fluids **28**, 2172 (1985).
[4]P. Terry and W. Horton, Phys. Fluids **25**, 491 (1982).
[5]J. Powers and P. B. Mumola, Plasma Phys. **13**, 817 (1971); Y. C. Kim, L. Khadra, and E. J. Powers, Phys. Fluids **23**, 2250 (1980).
[6]Lin I and Ming-Shing Wu, Phys. Lett. A **124**, 271 (1987).
[7]Lin I and Ming-Shing Wu, J. Appl. Phys. **62**, 4077 (1987).
[8]Y. Karamoto, Prog. Theor. Phys. Suppl. **64**, 346 (1978); Y. Oono and M. Kohmoto, Phys. Rev. Lett. **55**, 2927 (1985).
[9]H. T. Moon, P. Huerre, and L. G. Redekopp, Physica D **7**, 135 (1983).
[10]For example, H. L Swinney, Physica D **7**, 3 (1983).
[11]A. Brandstater, J. Swift, H. L. Swinney, A. Wolf, J. D. Farmer, E. Jen, and P. J. Crutchfield, Phys. Rev. Lett. **51**, 1442 (1983).
[12]G. A. Held and C. Jeffries, in *Dimension and Entropies in Chaotic Systems*, edited by G. Mayer-Kress (Springer, Berlin, 1986), p. 158; A. Brandstater, H. L. Swinney, and G. T. Chapman, in *ibid.*, p. 150.
[13]T. Yazaki, S. Takashima, and F. Mizutani, Phys. Rev. Lett. **58**, 1108 (1987).
[14]D. Rulle and F. Takens, Commun. Math. Phys. **20**, 167 (1971). S. Newhouse, D. Ruelle, and F. Takens, *ibid.* **64**, 35 (1978).
[15]S. Ciliberto and J. P. Gollub, Phys. Rev. Lett. **52**, 922 (1984); E. Meron and I. Procaccia, *ibid.*, **56**, 1323 (1986).
[16]Lin I, J. Appl. Phys. **58**, 2981 (1985); Lin I and Ming-Shing Wu, *ibid.* **60**, 1946 (1986).
[17]P. Grassberger and I. Procaccia, Phys. Rev. Lett. **50**, 346 (1983).